Article:
Wu, R., Navarro-Cia, M., Chekulaev, D. et al. (2023) Active control of mid-wavelength infrared non-linearity in silicon photonic crystal slab. Optics Express, 31 (22). 497371. pp. 35644-35652. ISSN: 1094-4087

https://doi.org/10.1364/oe.497371

Research Article | Vol. 31, No. 22 / 23 Oct 2023 / Optics Express 35644
Optics EXPRESS

Active control of mid-wavelength infrared non-linearity in silicon photonic crystal slab

RIHAN WU,[1] MIGUEL NAVARRO-CIA,[1,2] DIMITRI CHEKULAEV,[3] JACK COLLINS,[1] AND ANDREY KAPLAN[1,*]

[1]School of Physics and Astronomy, University of Birmingham, Birmingham, UK
[2]Department of Electronic, Electrical and Systems Engineering, University of Birmingham, Birmingham, UK
[3]Department of Chemistry, University of Sheffield, Sheffield S3 7HF, UK
*a.kaplan.1@bham.ac.uk

Abstract: Natural materials' inherently weak nonlinear response demands the design of artificial substitutes to avoid optically large samples and complex phase-matching techniques. Silicon photonic crystals are promising artificial materials for this quest. Their nonlinear properties can be modulated optically, paving the way for applications ranging from ultrafast information processing to quantum technologies. A two-dimensional 15-μm-thick silicon photonic structure, comprising a hexagonal array of air holes traversing the slab's thickness, has been designed to support a guided resonance for the light with a wavelength of 4-μm. At the resonance conditions, a transverse mode of the light is strongly confined between the holes in the "veins" of the silicon component. Owing to the confinement, the structure exhibits a ratio of nonlinear to linear absorption coefficients threefold higher than the uniform silicon slab of the same thickness. A customised time-resolved Z-scan method with provisions to accommodate ultrafast pump-probe measurements was used to investigate and quantify the non-linear response. We show that optically pumping free charge carriers into the structure decouples the incoming light from the resonance and reduces the non-linear response. The time-resolved measurements suggest that the decoupling is a relatively long-lived effect on the scale comparable to the non-radiative recombination in the bulk material. Moreover, we demonstrate that the excited free carriers are not the source of the nonlinearity, as this property is determined by the structure design.

1. Introduction

Silicon Photonic Crystals (SiPhCs) have attracted great attention in research and applications development because of their rich physics and potential to develop electro-optical devices which can be integrated into existing semiconductor technology. They exhibit the advantages of low fabrication cost, compatibility with silicon electronics production, and low signal attenuation over a broad spectral range below the electronic band-gap [1]. More broadly, there are demonstration of PhCs in light guiding [2,3], trapping [4,5], switching [6–8], lasing [9–11] and nonlinear applications [12,13].

Despite the extensive investigation on light manipulation with SiPhCs in telecom wavelengths, such as all-optical switches based on nanocavities [14], subwavelength nanowires with high switching contrast and speed [15], photon trapping and release that can be used in photonic circuits [16] and dispersion-compensation in fibres and nonlinear optics [17,18], only a few studies have been reported considering the Mid-Wavelength Infrared (MWIR, the spectral range covering the wavelength between 3 and 8 μm) region [19]. The main applications in this range are night-vision in civilian security, "heat-seeking" through the atmospheric window in defence, free-space communication and thermal imaging [20]. The advantage of using MWIR optics is

#497371 https://doi.org/10.1364/OE.497371
Journal © 2023 Received 12 Jul 2023; revised 6 Sep 2023; accepted 2 Oct 2023; published 10 Oct 2023

Optics EXPRESS

a low loss in the atmospheric window facilitating the propagation distance far more extended than for telecom and visible light wavelengths [21]. Imaging and rangefinding in MWIR are less affected by dust, fog, smoke and cloud because of more negligible scattering and absorption cross-sections than at shorter wavelengths. Therefore, this work explores aspects contributing to developing SiPhCs for light guiding and modulating in the MWIR spectral range.

There are three most common approaches to implement all-optical signal modulation by inducing modification to the optical response by either thermal, optical bistability or free carrier excitation [8]. The all-optical modulation has the advantage of rapid modulation speed, stable operation performance and high compatibility with other photonic devices over the conventional electronic and mechanical counterparts [22]. Thermal modulation is disadvantageous because of its slow switching speed and high energy consumption. Optical bistability utilises nonlinear optical effects such as two-photon absorption or Kerr lensing to modulate the incident light intensity, which relays on a material with significant nonlinear coefficients. In contrast, a free carrier injection is a straightforward approach for all-optical switching and modulation. It usually employs a laser pulse to excite the free carriers and change the material's optical response (transmittance/reflectance) at a wavelength of interest. The main drawback of this approach is that relatively high laser fluence is required. As shown in an approximate estimate of Supplemental Document, to achieve a 50% modulation contrast using crystalline silicon as the modulator material, at least 10^{19} cm^{-3} free carrier density is required, necessitating to use of a milli-Joule per square centimetre of the pump fluence. The modulation contrast is only fractionally improved by reducing the amount of the reflected light in 2D periodic structures pumped by the similar fluences [8,23]. This problem requires a more sophisticated approach to employ structures that can trap the light at specific conditions and induce nonlinear response [24,25]. Therefore, we focus on a nonlinear optical regime attempting to achieve the same modulation contrast but with a lower pump intensity. To improve the performance, bulk materials need to be modified with methods such as surface passivation [26] or engineering structures such as ring cavity [27,28], SiPhCs [29,30] and metasurfaces [31,32].

In this work, we designed a two-dimensional (2D) SiPhC structure that supports Fano-like resonance at the wavelength of ~4 μm in the MWIR region. We show that at the resonance condition, a non-linear absorption of the SiPhC is strongly enhanced compared to a uniform crystalline silicon slab with the same thickness. We employed an optical pump to inject free carriers of the moderate density of 10^{18} cm^{-3} to implement optical modulation. This shifts the resonance to a different photonic band to which coupling is suppressed. The incoming light is partially rejected back into the environment, diminishing the amount of light absorbed non-linearly. This rejection is associated with a large imaginary part related to the free carriers induced by the pump. Such a combination of the carrier injection and optical bistability remarkably reduced the pump intensity requirement to modulate signal traversing the slab. We demonstrate that achieving 50% of the absorption modulation contrast requires a pump intensity of an order magnitude less than operating in the linear regime or using a uniform silicon slab.

For this demonstration, we designed a time-resolved pump-probe Z-scan setup to explore the nonlinear response of SiPhC and its evolution in time following ultrafast excitation. In our set-up, instead of the traditional translating of the sample through the focusing point of the signal beam [33,34], we move the focusing lens while keeping the sample position stationary. This modification allows us to investigate the SiPhC nonlinearity with and without the pump.

2. Pump-probe time-resolved Z-scan set-up

Figure 1 shows the pump-probe Z-scan setup that we employed in this work. An intensive pump beam was generated by a femtosecond (fs) laser system delivering pulses of 60 fs duration at a 1 kHz repetition rate. The pump wavelength was centred around 800 nm to excite free carriers above the electronic band gap of SiPhC. The MWIR 4 μm probe pulses of ~100 fs at

Optics EXPRESS

the same repetition rate were generated by a Nonlinear Optical Parametric Amplifier. Using a beam profiler, the pump and probe beam diameters were determined by measuring the beam's intensity distribution at the sample location. The arrival time difference between the pump and probe pulses on the SiPhC surface was controlled by varying the optical path length of the pump passing through a retroreflector located on a computer-controlled motorised Stage 2. Stage 1, which carried the lens controlling the focusing of the probe at the SiPhC surface, was placed in the probe's optical path.

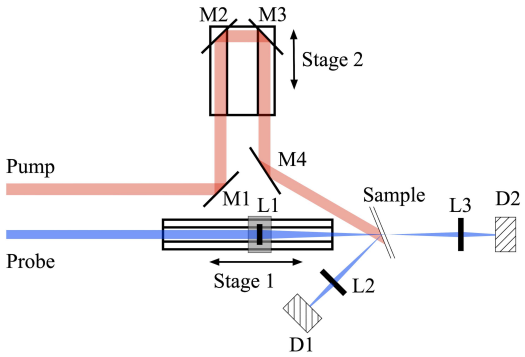

Fig. 1. The pump-probe Z-scan setup developed for investigation of time-resolved non-linear properties of thin slabs. The pump and probe have a wavelength of 800 nm and 4 μm, respectively. Two computer-controlled motorised stages are used: Stage 2 controls the arrival time difference between pump and probe pulses on the sample surface. Stage 1 carries a focusing lens (L1, f=100mm) which controls the focusing condition of the probe beam at the sample surface. The reflected and transmitted light of the sample are collected by two lenses (L2 and L3, both with f=150mm) in front of two MCT detectors (D1 and D2).

To focus the MWIR 4 μm probe pulses, the Z-scan set-up incorporated a Germanium-Plano-Convex lens with a focal length of 100 mm mounted onto a translational stage to modify the focusing conditions at the sample in a controlled manner. The beam diameter measured before passing through the lens was 5 mm, while it was approximately 100 um at the focus. Maintaining the pump beam consistently larger than the probe at the sample surface was paramount to guarantee an almost spatially homogenous excitation over the probe area during the translation process of the probe lens. As such, no lens was used in the pump beam path. The diameter of the pump beam was measured to be around 10 mm, twice larger than the unfocused probe beam diameter.

The sample was tilted to 20° concerning the probe beam incidence angle, while that angle for the pump beam was 30°. To ensure a nearly spatially homogeneous excitation across the probe beam, the pump beam spot diameter on the sample was adjusted to be a few times larger. The effect of tilting the sample produces somewhat elliptical beam profiles of the probe and pump. To minimize this effect, we kept the pump and probe angles very close to each other. The ratio between the minor and major axes is about 0.9 for the probe beam, while for the pump is 0.75. The non-identical intensity distribution along those axes might introduce some degree of birefringence. However, the experiment cannot discern this as the detector integrates the signal over the entire area. Rotating half-wave plates controlled both the pump and probe intensities in front of linear polarisers, which also set the beam polarisation. The probe beam was p-polarised to match the coupling symmetry required to excite the fourth TM mode of the SiPhC slab, while TE modes are ruled out because of polarisation. The coupling is facilitated by the matching conditions provided by the slab orientation and mode broadness due to imperfections. The angle of incidence and wavelength determines a single point in the dispersion diagram. This point is

Optics EXPRESS

centred on the eigen solution of the fourth TM mode only. Although an angular distribution of the probe beam on the surface of the slab might provide a partial excitation of the third mode, but its contribution is only fractional.

This arrangement differs from the conventional Z-scan method, where a sample is placed on the stage that translates it through the focal point of a fixed lens. However, the traditional approach is impractical for the pump-probe experiments since the pump position would shift on the sample surface while it moves through the probe's focus. Defocussing the pump beam to a large enough spot to cover the entire surface will not solve the problem. A spatial intensity distribution of the pump would result in the variation of the excitation profile on the surface. Therefore, our approach is to fix the sample and translate the focusing lens of the probe. We verified the reliability of our system by performing the Z-scan measurements without the pump in both configurations and confirmed that the results were identical for an open aperture. Yet, this approach still has limitations for the closed-aperture modality and was not used in this work. We only performed the open-aperture Z-scan experiments by collecting both the transmitted and reflected light through two lenses in front of two MCT detectors. A pair of preamplifiers and a lock-in amplifier (Zurich Instruments) were connected to the detectors, and the data was read out and processed by LabVIEW software. We have carefully verified that all the light has been collected by the detectors while scanning the focusing of the probe.

3. 2D silicon photonic crystal structure

The sub-wavelength structured SiPhC membranes were made by photoelectrochemical etching of silicon in HF using a procedure similar to that described elsewhere [35]. In this procedure, an ordered hexagonal 2D array of holes was etched through a 15-μm-thick slab of bulk silicon. The lattice constant and hole diameter were 1.5 and 1 μm, respectively, as shown in the inset of Fig. 2(a). The samples are free-standing membranes glued to a metal washer-like holder with an inner open diameter of 1 cm. This arrangement is viable for silicon-based materials, as they possess the strength for this support method.

We designed a 2D SiPhC structure that supports a Fano-type resonance at 4 μm, in which a narrow Bragg band of a TM mode interacts constructively or destructively with a continuum spectrum [36]. At the resonance, the light incoming from the environment is coupled to the mode and is channelled through the structure. A band diagram in a reduced zone scheme is plotted in Fig. 2(a) and corresponds to the structure geometry shown in the inset. The blue dots indicate TM-guided modes, while the black line marks the light cone. The green dashed line designates tilting to 20° when the plane of incidence is oriented along the $\Gamma - K$ direction. The red dashed line corresponds to the probe's frequency. The guided modes intersecting the light cone can be coupled to an external light source, directing the light between the structure and the environment. Yet, these modes can retain a portion of electromagnetic power within the structure. According to our experimental conditions, the fourth mode is coupled to the probe light as denoted by the intersection of green and red dashed lines with that mode. The calculation details can be found in the Supplemental Document. Moreover, the presence of the guided resonances was confirmed by measuring the transmittance spectrum and observing the intensity drop at the frequencies corresponding to the guided resonances, see Fig. S1 of Supplemental Document.

Figure 2(c) shows the spatial distribution of the electric field of the fourth mode exhibiting the confinement in the silicon "veins" of the SiPhC slab. When this mode interacts with the continuum spectrum in the surrounding, a Fano-type resonance is expected to occur. Light can be channelled through the slab interacting with the medium in the areas of the field confinement. For a material exhibiting non-linear absorption, more light will be absorbed in the areas where the field is confined. On average, more light will be absorbed in the photonic structure than in a uniform slab where light is delocalised.

Optics EXPRESS

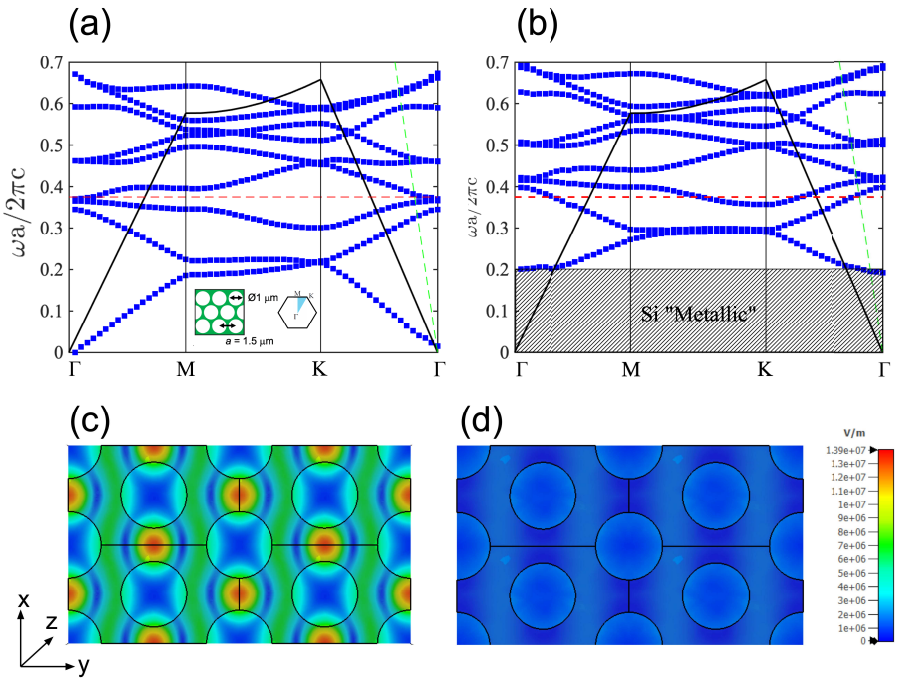

Fig. 2. (a) The band structure of TM modes for 2D SiPhC. The dashed red and green lines indicate the probe light's normalised frequency and the cone of the incoming light. The inset shows the 2D SiPhC structure in real space and the corresponding first 2D Brillouin zone. The black line indicates the light cone at the normal incidence. (b) The band structure of the 2D SiPhC injected with the free carriers by 800 nm and 0.7 mJ/cm^2 pump. (c), (d) top views of the electric field distribution in the middle cross-section of the SiPhC slab for unpumped and pumped cases, respectively.

The situation changes when the structure is optically injected with the free carriers. Figure 2(b) shows the band structure of the same 2D SiPhC but excited by the pump fluence of 0.7 mJ/cm^2 injecting the free carriers density of 10^{18} cm^{-3}. The lower energy Bragg modes are distorted and shifted upwards. Below the first band, the structure became metallic with no supported modes. Because of the shift, the external light is supposed to be guided through via interaction with the second band. Yet, Fig. 2(d) suggests that the coupling is suppressed as the field intensity is weaker by order of magnitude than for the unpumped structures. Here, the light is strongly reflected at the air - SiPhC interface because of the partly metallic properties of the band, which is characterised by a significant imaginary part ($\varepsilon_{imaginary} \sim 1$) of the effective dielectric function.

Thus, the coupling of the external light into the SiPhC slab can be toggled on or off by pumping the free carriers optically. For the unpumped sample, the light is confined and guided through the veins, where it is absorbed predominantly non-linearly. Hence, the modulation can be realised between two states of non-linear absorption and light rejection for the unpumped and pumped structures, respectively.

4. Results and discussion

To verify the enhancement of the SiPhC slab nonlinear response, we performed the Z-scan measurements (in the absence of the pump) and compared them to a reference uniform silicon slab of the same thickness. From the simultaneous recording of the reflectance, R, and transmittance, T, signals, the absorptance, $A = 1 - R - T$, can be directly obtained. The comparison of

Optics EXPRESS

the normalised absorptance, A/A_0, between the two samples is shown in Fig. 3(a). Here, A_0 is linear absorptance measured for a loosely focused beam, while A is a function of the sample distance from the focal point. At the focus, $z = 0$, the nonlinear absorption process enhances the absorptance of the uniform silicon slab by $\sim 30\%$, while it doubles for the SiPhC slab. We note the importance of recording both the transmitted and reflected intensity for the Z-scan measurements of thin opaque materials exhibiting Fabry-Pérot fringes. Monitoring the transmittance or reflectance solely might complicate the deconvolution of linear and non-linear responses.

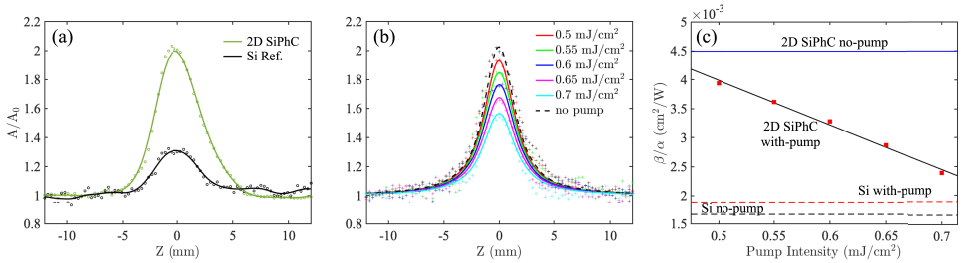

Fig. 3. (a) Comparison of the Z-scan normalised absorptance, A/A_0, of 4 μm wavelength for the 15-μm-thick uniform silicon (Si ref) and SiPhC slabs, both are 15 μm-thick; (b) the Z-scan for SiPhC slab, pumped by loosely focused 800 nm beam of different fluences; the dashed line represents the measurement in the absence of the pump; (c) The ratio of non-linear, β, to linear, α absorption coefficients as a function of the pump fluence. The solid blue line indicates the ratio limit for the unpumped sample. The dashed lines signify the span of the ratio range between unpumped and pumped uniform silicon.

In the next stage, we investigated the optical response when the samples were injected optically with the free carriers. Note the absorption of the pump is a linear process involving phonon assistance. The process is well understood and tabulated in the literature, see [32] for example. As demonstrated in Fig. 2(b) and (d), under pumping, the resonance is shifted to the second photonic band but poorly coupled because the carriers induce a large imaginary part, and the incoming light is reflected back. The Z-scan was performed for the pump fluence in the range between 0.5 and 0.7 mJ/cm^2 corresponding to the carrier density of 7×10^{17} and 10^{18} cm^{-3}, respectively, to show a gradual decoupling from the guided resonance and the decrease of non-linear response. Indeed, Fig. 3(b) shows that the increase of the pump fluence reduces the amount of infrared light propagating and, consequently, non-linearly absorbed within the sample.

To further clarify the physical picture of the process, the Z-scan waveforms were analysed by the method described elsewhere [34,37] to retrieve the ratio of the linear, α, to the non-linear, β, absorption coefficients. Figure 3(c) shows that this ratio monotonically drops as a function of the pump fluence, approaching the response of the silicon slab. On the low fluence end, the beta/alpha line crosses the no-pump line around 0.42 mJ/cm^2. This value can be considered an apparent threshold for observing the non-linear response. Thus, the non-linear response diminishes as the free carriers' injection decouples the incoming probe light from the guided resonance. We note the linear behaviour of β/α as a function of pump fluence is an empirical observation. There is no formula or a short-cut calculation to calculate this. The nature of the enhancement is rather complex and requires the calculation of non-linear propagation through the slab, a task beyond the scope of this work.

Figure 3(c) also shows that the response range of the uniform silicon slab for the same conditions is much narrower, and the trend is the opposite, where the non-linearity increases with the pump fluence.

Optics EXPRESS

The effect of the free carriers on the non-linear response is generally considered short-lived. It tends to fade within a few hundred femtoseconds as soon the carriers thermalise following the excitation [38,39]. Such a fast response is desirable for optical switching but unsustainable in photodetecting devices relying on the high carrier density in steady-state conditions. Therefore, developing a SiPhC slab for electro-optical applications requires an evaluation of the time-resolved properties.

We performed a time-resolved pump-probe experiment with the SiPhC slab positioned at the distance of the strongest and weakest non-linear response, $Z = 0$ and $Z = 12$ mm, from the lens' focus, respectively. Figure 4 shows the time-resolved *fractional* absorptance change, $\Delta A/A_{no-pump}$, as a function of the arrival time difference, Δt, between the pump and probe pulses on the sample surface, where $\Delta A = A(t) - A_{no-pump}$, with $A(t)$ designating the absolute absorptance at time t and $A_{no-pump}$ is the absolute absorptance in the pump's absence. It can be seen that a fast component around the zero delay, which is usually associated with the non-linear response of the free carriers, is absent in both cases, and the decay is nearly identical. Thus, we conclude that the nonlinearity is a property of the structure design to which the injected free carriers do not contribute directly. Otherwise, we would see the fast component at the tight focusing of $Z = 0$. Moreover, the observed carrier decay time is much longer than a few hundred picoseconds, resembling the non-radiative carrier decay in bulk silicon. This proposes that the fundamental electronic properties related to the carriers' recombination are similar in bulk and structured silicon.

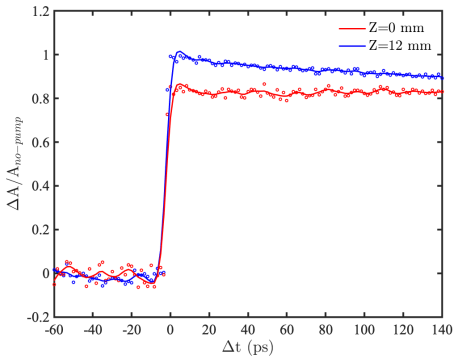

Fig. 4. Fractional change of the absorptance, $\Delta A/A_{no-pump}$, as a function of the arrival time difference between the pump and probe pulses, Δt, when SiPhC slab is positioned in (red) and out (blue) of the focus, $Z = 0$ and $Z = 12$ mm, respectively. The pump fluence is 0.7 mJ/cm^2.

In addition, we investigated whether possible heating induced by the pump is affecting the non-linear response. For this, a series of Z-scan experiments were performed, with the pump arriving before or after the probe. When the probe arrives before the pump, it propagates through the sample before the free carriers are excited, and thus, it is not affected directly by them. However, the carriers decay in between the pump pulses and might induce residual heat, which can be accumulated in the crystal lattice. The Z-scan absorptance measurements shown in Fig. 2(S) of the Supplemental Document demonstrate that the effect of heating on the non-linearity can be ruled out. The Z-scan absorptance, with the pump arriving after the probe, remains nearly identical to that recorded without the pump, shown in the main text in Fig. 3(a). Moreover, the results shown in Fig. 2(S) of the Supplemental Document demonstrate qualitatively that the change of the nonlinearity is related to free carriers injection only.

Optics EXPRESS

5. Conclusions

In conclusion, we designed a 2D SiPhC structure that supports a Fano-type guided resonance at 4 μm wavelength. The electric field is strongly confined in silicon "veins" at the resonance conditions, and the structure exhibits an enhanced non-linear response. Using a customised Z-scan method, we demonstrate that non-linear absorption contributes to doubling the total absorptance of SiPhC slab at the focus. The Z-scan waveform analysis revealed that the ratio β/α of the non-linear to linear absorption coefficients is 4.5×10^{-3} cm^2/W for the SiPhC slab as opposed to 1.7×10^{-3} cm^2/W for the silicon slab. The time-resolved experimental results propose that the non-linear effect is a property of the structures, while the electronic properties remain unchanged. However, the injection of the free carriers modifies the optical bands' structure, causing the resonance's coupling to decrease and diminishing the nonlinear effect. Nevertheless, the electronic properties governing the carriers' decay remain similar to that of the bulk material, unaffected by the modified optical nonlinearity.

Funding. European Union Horizon 2020 (777714); Engineering and Physical Sciences Research Council (EP/V000055/1).

Acknowledgments. J.C. thanks Dstl for the financial support enabled by the grant DSTLX100099482. M.N.-C. acknowledges support from European Union Horizon 2020 research and innovation programme (Grant No. 777714). A.K. thanks the Engineering and Physical Sciences Research Council for financial support (Grant number EP/V000055/1; Metal Atoms on Surfaces and Interfaces for Sustainable Future).

Disclosures. The authors declare no conflicts of interest.

Data availability. Data underlying the results presented in this paper are not publicly available at this time but may be obtained from the authors upon reasonable request.

Supplemental document. See Supplement 1 for supporting content.

References

1. S. Yan, X. Zhu, L. H. Frandsen, S. Xiao, N. A. Mortensen, J. Dong, and Y. Ding, "Slow-light-enhanced energy efficiency for graphene microheaters on silicon photonic crystal waveguides," Nat. Commun. **8**(1), 14411 (2017).
2. Y. Jiang, W. Jiang, L. Gu, X. Chen, and R. T. Chen, "80-micron interaction length silicon photonic crystal waveguide modulator," Appl. Phys. Lett. **87**(22), 221105 (2005).
3. C. Monat, C. Grillet, M. Collins, A. Clark, J. Schroeder, C. Xiong, J. Li, L. O'faolain, T. F. Krauss, and B. J. Eggleton, "Integrated optical auto-correlator based on third-harmonic generation in a silicon photonic crystal waveguide," Nat. Commun. **5**(1), 3246 (2014).
4. S. Bhattacharya and S. John, "Photonic crystal light trapping: Beyond 30% conversion efficiency for silicon photovoltaics," APL Photonics **5**(2), 020902 (2020).
5. S. B. Mallick, M. Agrawal, and P. Peumans, "Optimal light trapping in ultra-thin photonic crystal crystalline silicon solar cells," Opt. Express **18**(6), 5691–5706 (2010).
6. T. Tanabe, K. Nishiguchi, A. Shinya, E. Kuramochi, H. Inokawa, M. Notomi, K. Yamada, T. Tsuchizawa, T. Watanabe, and H. Fukuda, "Fast all-optical switching using ion-implanted silicon photonic crystal nanocavities," Appl. Phys. Lett. **90**(3), 031115 (2007).
7. J. Li, J. He, and Z. Hong, "Terahertz wave switch based on silicon photonic crystals," Appl. Opt. **46**(22), 5034–5037 (2007).
8. R. Wu, J. Collins, D. Chekulaev, and A. Kaplan, "All-optical modulation and ultrafast switching in mwir with sub-wavelength structured silicon," Appl. Sci. **9**(9), 1808 (2019).
9. A. Tandaechanurat, S. Ishida, D. Guimard, M. Nomura, S. Iwamoto, and Y. Arakawa, "Lasing oscillation in a three-dimensional photonic crystal nanocavity with a complete bandgap," Nat. Photonics **5**(2), 91–94 (2011).
10. M. Nomura, S. Iwamoto, K. Watanabe, N. Kumagai, Y. Nakata, S. Ishida, and Y. Arakawa, "Room temperature continuous-wave lasing in photonic crystal nanocavity," Opt. Express **14**(13), 6308–6315 (2006).
11. A. Yokoo, M. Takiguchi, M. D. Birowosuto, K. Tateno, G. Zhang, E. Kuramochi, A. Shinya, H. Taniyama, and M. Notomi, "Subwavelength nanowire lasers on a silicon photonic crystal operating at telecom wavelengths," ACS Photonics **4**(2), 355–362 (2017).
12. A. Ghanbari, A. Kashaninia, A. Sadr, and H. Saghaei, "Supercontinuum generation with femtosecond optical pulse compression in silicon photonic crystal fibers at 2500 nm," Opt. Quantum Electron. **50**(11), 411 (2018).
13. M. Galli, D. Gerace, K. Welna, T. F. Krauss, L. O'Faolain, G. Guizzetti, and L. C. Andreani, "Low-power continuous-wave generation of visible harmonics in silicon photonic crystal nanocavities," Opt. Express **18**(25), 26613–26624 (2010).
14. T. Tanabe, M. Notomi, S. Mitsugi, A. Shinya, and E. Kuramochi, "All-optical switches on a silicon chip realized using photonic crystal nanocavities," Appl. Phys. Lett. **87**(15), 151112 (2005).

Optics EXPRESS

15. M. Takiguchi, N. Takemura, K. Tateno, K. Nozaki, S. Sasaki, S. Sergent, E. Kuramochi, T. Wasawo, A. Yokoo, and A. Shinya, "All-optical inasp/inp nanowire switches integrated in a si photonic crystal," ACS Photonics **7**(4), 1016–1021 (2020).
16. Q. Gan, Y. J. Ding, and F. J. Bartoli, "Rainbow trapping and releasing at telecommunication wavelengths," Phys. Rev. Lett. **102**(5), 056801 (2009).
17. T. Matsui, K. Nakajima, and I. Sankawa, "Dispersion compensation over all the telecommunication bands with double-cladding photonic-crystal fiber," J. Lightwave Technol. **25**(3), 757–762 (2007).
18. K. Saitoh and M. Koshiba, "Highly nonlinear dispersion-flattened photonic crystal fibers for supercontinuum generation in a telecommunication window," Opt. Express **12**(10), 2027–2032 (2004).
19. A. Zakar, S. J. Park, V. Zerova, A. Kaplan, L. T. Canham, K. L. Lewis, and C. D. Burgess, "MWIR optical modulation using structured silicon membranes," in *Emerging Imaging and Sensing Technologies*, vol. 9992 K. L. Lewis and R. C. Hollins, eds., International Society for Optics and Photonics (SPIE, 2016), p. 999203.
20. J. Collins, R. Wu, A. Davie, and A. Kaplan, "All-optical modulator for gated range finding and active imaging in lwir," in *Electro-Optical and Infrared Systems: Technology and Applications XVII*, vol. 11537 (International Society for Optics and Photonics, 2020), p. 115370L.
21. R. Wu, J. Collins, C. D. Burgess, R. A. Lamb, and A. Kaplan, "Demonstration of time-of-flight technique with all-optical modulation and mct detection in swir/mwir range," in *Emerging Imaging and Sensing Technologies for Security and Defence III; and Unmanned Sensors, Systems, and Countermeasures*, vol. 10799 (International Society for Optics and Photonics, 2018), p. 1079904.
22. S. J. Park, A. Zakar, V. L. Zerova, D. Chekulaev, L. T. Canham, and A. Kaplan, "All-optical modulation in mid-wavelength infrared using porous si membranes," Sci. Rep. **6**(1), 30211 (2016).
23. D. Chekulaev, V. Garber, and A. Kaplan, "Free carrier plasma optical response and dynamics in strongly pumped silicon nanopillars," J. Appl. Phys. **113**(14), 143101 (2013).
24. K. Q. Le and S. John, "Synergistic plasmonic and photonic crystal light-trapping: Architectures for optical up-conversion in thin-film solar cells," Opt. Express **22**(S1), A1–A12 (2014).
25. S. Mandal, X. Serey, and D. Erickson, "Nanomanipulation using silicon photonic crystal resonators," Nano Lett. **10**(1), 99–104 (2010).
26. Y. Kim, J. Han, M. Takenaka, and S. Takagi, "Low temperature al 2 o 3 surface passivation for carrier-injection sige optical modulator," Opt. Express **22**(7), 7458–7464 (2014).
27. Q. Xu, S. Manipatruni, B. Schmidt, J. Shakya, and M. Lipson, "12.5 gbit/s carrier-injection-based silicon micro-ring silicon modulators," Opt. Express **15**(2), 430–436 (2007).
28. B. R. Moss, C. Sun, M. Georgas, J. Shainline, J. S. Orcutt, J. C. Leu, M. Wade, Y.-H. Chen, K. Nammari, and X. Wang, "A 1.23 pj/b 2.5 gb/s monolithically integrated optical carrier-injection ring modulator and all-digital driver circuit in commercial 45nm soi," in *2013 IEEE International Solid-State Circuits Conference Digest of Technical Papers*, (IEEE, 2013), pp. 126–127.
29. L. Gu, W. Jiang, X. Chen, L. Wang, and R. T. Chen, "High speed silicon photonic crystal waveguide modulator for low voltage operation," Appl. Phys. Lett. **90**(7), 071105 (2007).
30. A. Haché and M. Bourgeois, "Ultrafast all-optical switching in a silicon-based photonic crystal," Appl. Phys. Lett. **77**(25), 4089–4091 (2000).
31. A. Krasnok, M. Tymchenko, and A. Alù, "Nonlinear metasurfaces: a paradigm shift in nonlinear optics," Mater. Today **21**(1), 8–21 (2018).
32. H. Aouani, M. Navarro-Cía, M. Rahmani, and S. A. Maier, "Unveiling the origin of third harmonic generation in hybrid ito–plasmonic crystals," Adv. Opt. Mater. **3**(8), 1059–1065 (2015).
33. M. Sheik-bahae, A. A. Said, and E. W. V. Stryland, "High-sensitivity, single-beam n2 measurements," Opt. Lett. **14**(17), 955–957 (1989).
34. R. Wu, J. Collins, L. T. Canham, and A. Kaplan, "The influence of quantum confinement on third-order nonlinearities in porous silicon thin films," Appl. Sci. **8**(10), 1810 (2018).
35. J. Schilling, R. Wehrspohn, A. Birner, F. Müller, R. Hillebrand, U. Gösele, S. Leonard, J. Mondia, F. Genereux, and H. Van Driel, "A model system for two-dimensional and three-dimensional photonic crystals: macroporous silicon," J. Opt. A: Pure Appl. Opt. **3**(6), S121–S132 (2001).
36. U. Fano, "Effects of configuration interaction on intensities and phase shifts," Phys. Rev. **124**(6), 1866–1878 (1961).
37. M. Dinu, F. Quochi, and H. Garcia, "Third-order nonlinearities in silicon at telecom wavelengths," Appl. Phys. Lett. **82**(18), 2954–2956 (2003).
38. M. Z. Alam, I. De Leon, and R. W. Boyd, "Large optical nonlinearity of indium tin oxide in its epsilon-near-zero region," Science **352**(6287), 795–797 (2016).
39. S. Peruch, A. Neira, G. A. Wurtz, B. Wells, V. A. Podolskiy, and A. V. Zayats, "Geometry defines ultrafast hot-carrier dynamics and kerr nonlinearity in plasmonic metamaterial waveguides and cavities," Adv. Opt. Mater. **5**(15), 1700299 (2017).